

## Supplementary Information

### Self-powered ultrasensitive and highly stretchable temperature-strain sensing composite yarns

*Kening Wan, Yi Liu, Giovanni Santagiuliana, Giandrin Barandun, Prospero Taroni Junior, Firat Güder, Cees W.M. Bastiaansen, Mark Baxendale, Oliver Fenwick, Dimitrios G. Papageorgiou, Steffi Krause, Han Zhang, Emiliano Bilotti\**

Dr. K. Wan, Dr. G. Santagiuliana, Prof. C. W. M. Bastiaansen, Dr. O. Fenwick Dr. D. G. Papageorgiou, Dr. S. Krause, Dr. H. Zhang, Dr. E. Bilotti  
School of Engineering and Materials Science, Queen Mary University of London, Mile End Road, London, E1 4NS, U.K.  
E-mail: e.bilotti@qmul.ac.uk

Dr. Y. Liu  
Department of Materials, Loughborough University, Loughborough, LE11 3TU, U.K.

Dr. G. Santagiuliana, Dr. H. Zhang, Dr. E. Bilotti  
Nanoforce Technology Ltd., Joseph Priestley Building, Queen Mary University of London, Mile End Road, London, E1 4NS, U.K.

G. Barandun, Dr. F. Güder  
Department of Bioengineering, Imperial College London, London SW7 2AZ, U.K.

Dr. P. T. Junior  
Institute for Materials Discovery, University College London, Malet Place, London WC1E 7JE, UK

Prof. C. W. M. Bastiaansen  
Laboratory of Functional Organic Materials and Devices, Eindhoven University of Technology, P.O. Box 513, 5600 MB Eindhoven, The Netherlands

Dr. Mark Baxendale  
School of Physics and Astronomy, Queen Mary University of London, Mile End Road, London, E1 4NS, U.K.

## **Author contributions**

K.W. performed all the experimental works on yarn fabrication, devices fabrication, characterizations and data analysis. K.W. and Y.L. performed the smart glove sensing measurements with help from G.S.. K.W. and G.B. performed the wireless sensing fabrication and measurements after discussion with F.G. and E.B.. K.W. and P.T.G. performed the water stabilization measurements. Yarns fabrication was discussed with H.Z., interfacial shear strength and thickness calculation was discussed with D.G.P. and E.B.. Impedance analysis and equivalent circuit fitting were discussed with S.K. and E.B. and suggested by M.B.. This work was ideated and supervised by E.B. The paper was written with contributions from all authors with suggestions by C.W.M.B. and O.F..

## Methods

### Materials and fabrication:

Lycra<sup>®</sup> *Invista* yarns purchased from *Dupont* were washed by soap, acetone and isopropanol in sequence, in order to remove surface dust and oil. After drying at 80 °C in the oven, yarns were dipped into anhydrous DMSO (> 99.9 %, *Sigma Aldrich*) at 50 °C for 10 minutes, followed by dipping into PEDOT:PSS (*Clevios PHI1000, Heraeus GmbH*) with 10% DMSO solution for 5 minutes. The swelling process was inspired by our earlier work<sup>1</sup> while the conditions for current study were chosen by experiments. The swelling level is controlled by the dipping time in DMSO, and the optimized condition when DMSO have just infiltrated into the whole yarns has been chose. After the coating procedure, the yarns were fully dried at 120 °C in the oven for 5 hours not only to evaporate all the solvent, but also to anneal the yarns. The PEDOT:PSS coated yarn, named PY, was obtained after the as-mentioned procedures and cut into specimens with 20 mm length for the measurements. Cracked PEDOT:PSS coated yarn (CPY) was fabricated by stretching PY to 5%, 10%, 20%, 30%, 40%, 50%, 80%, 100%, 300%, 1000% and named as CPY-5, CPY-10, CPY-20, CPY-30, CPY-40, CPY-50, CPY-80, CPY-100, CPY-300, CPY-1000, respectively. If not mentioned specifically, the CPY-300 sample was used during the experimental procedures.

Self-powered single yarn strain sensor was fabricated with electrodes attached on both ends of the CPY by tying thin copper wire knots. Carbon grease was applied to eliminate contact resistance.

### Characterizations:

Optical microscopy images were obtained by an Olympus BX60 microscope equipped with an Olympus SC100 digital camera in reflection mode. Scanning electron microscopy (SEM) (*FEI Inspector-F*) was used to examine the morphology of the PEDOT:PSS coated layer with 3 kV acceleration voltage. For the evaluation of the cross-section, samples were cryo-fractured under liquid nitrogen and sputtered with gold to inhibit nonconductive Lycra<sup>®</sup> charging electrons.

The 2-point probe method was used to measure the electrical resistance of PYs and CPYs. A step voltage was applied by *Agilent 6614* DC power supply with the current measured by a *Keithley 6485* picoammeter simultaneously. The unit resistance of 1 cm length PY was measured and average value was taken from 30 specimens. Resistivity change with temperature was obtained with a tabletop probe station (*PS-100, Lakeshore*) equipped with a semiconducting parameter analyser (*Keithley, 4200SCS*) and a temperature controller (*Model 336, Lakeshore*).

Impedance spectra were measured by *Keysight E4980A* with four-terminal pair configuration in the frequency range of 20 Hz to 10 MHz. Two ends of PY were fixed on a frame with the distance between measured by a caliper. Copper wire electrodes were connected to the PY by knots with carbon grease paste, and the PY length between the two electrodes was approximately 10 mm at 0% strain.

The Seebeck coefficient of ~5 mm long segments PY was measured by the SB1000 Seebeck Measurement System equipped with a K20 Programmable Temperature Controller (*MMR Technologies Inc.*). A thermal load of approximately 1–2 K has been used together with a constantan wire as an internal reference.

The open circuit voltage was measured by a Keithley 2000 Multimeter. The power output was measured by connecting the PY/device with a variable resistor (range from 9  $\Omega$  to 999 M $\Omega$ ) to measure voltage and current simultaneously.

Tensile strains on fabricated strain sensor were applied by a quasi-static tensile tester (*Instron 5566*). The resistance change during stretching for a single yarn strain sensor was measured with an *Agilent 34401A* 6½ digital multimeter.

A bespoke humidity controller was set up for humidity tests. 0.6 L min<sup>-1</sup> different moist nitrogen gas was flow into a ~700 cm<sup>3</sup> chamber which takes ~ 600 s for stabilization. A humidity sensor (Fisher brand) was used for calibration.

For the wireless strain sensor demonstration, CPY was attached to the joint of index finger and the finger movements were detected by the resistance change of the yarn. A Bluetooth Low Energy module (BLE, *Adafruit Feather nRF52 Bluefruit LE*) based on a Nordic chip (*nRF52832*) was used to read the voltage (V) on an analog-to-digital converter. The electrical resistance of the CPY sensor ( $R_s$ ) were calculated based on the reference resistor ( $R_{ref}$ ) in BLE by  $R_s = (3.3/V) * R_{ref} - R_{ref}$ . And the data was sent to a smartphone via BLE and plotted in real-time.

For the self-powered strain sensor demonstration, a heater pad (*RS, 12 V dc, 7.5 W, item 245-556*) was attached to one end of the PY for temperature controlling and the other end stayed at room temperature to introduce temperature gradients. The picoammeter (*Keithley 6485*) was used for measuring output currents.

For the self-powered temperature (gradient) sensor, a controllable temperature was applied at one side by a commercial thermoelectric module. The actual temperature was measured by a thermal couple. For example, actual temperatures of 29°C, 46 °C and 67 °C has been obtained for the temperature difference of 7K, 24K and 45K, respectively. The voltage signal was collected by the multimeter (*Keithley 2000*) in real time. The voltage output under different strains was measured in a static method, where a certain strain was hold by the quasi-static tensile tester (*Instron 5566*). The same set up for temperature gradient controlling as for the self-powered sensor has been used, i.e., a commercial thermoelectric module being applied at one side of the yarn. The open circuit voltage was measured by a Keithley 2000 Multimeter by directly connected to the 2 ends of the yarn.

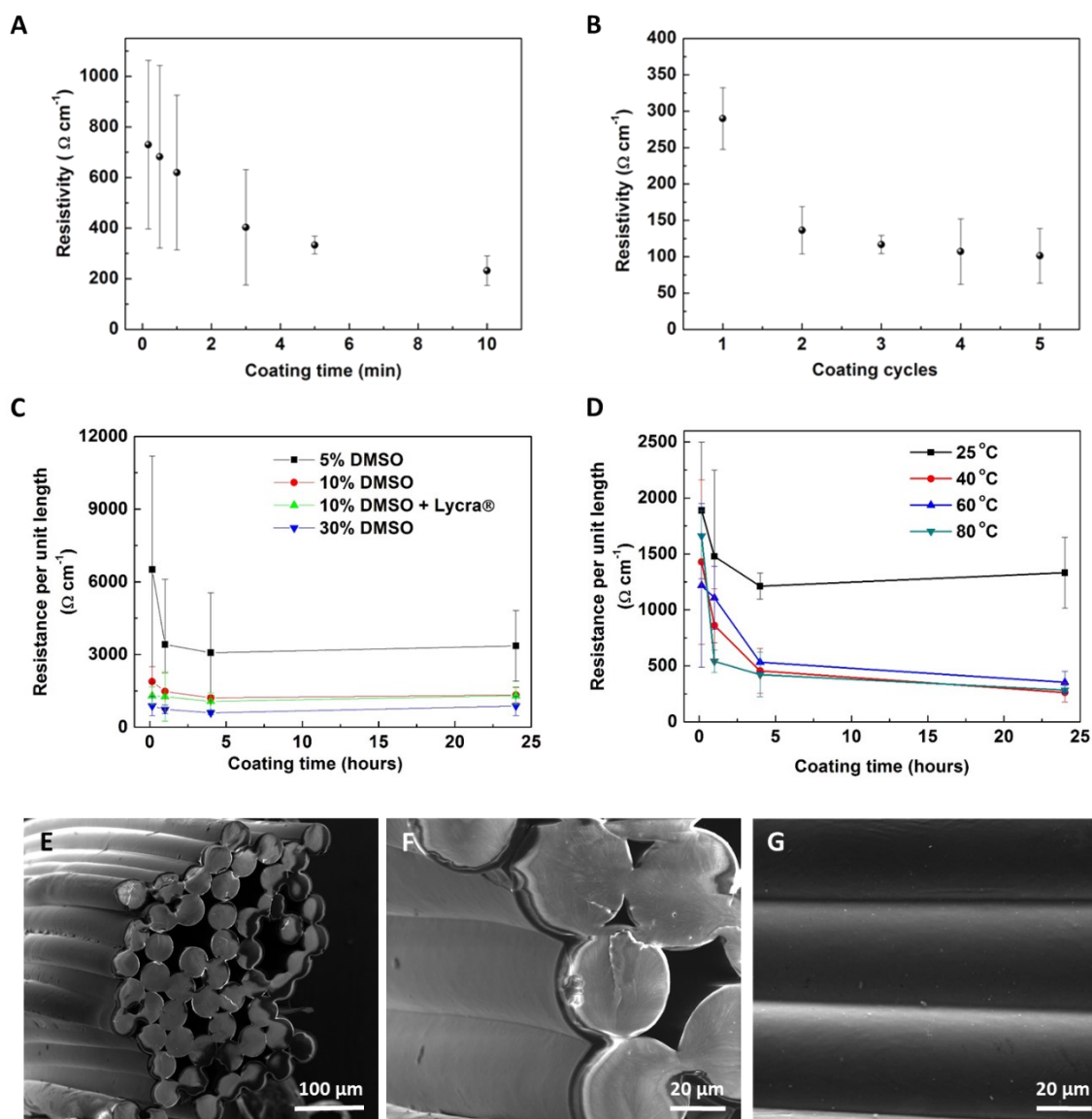


**Figure S1. Morphology and electrical properties of PEDOT:PSS coated Lycra® yarn by tow methods.** The effect of (A) coating time and (B) coating cycle to electrical resistivity by swell-coating method. The effect of (C) coating solution content and (D) coating temperature to resistivity with coating time for the original dip-coating method, i.e., without swelling procedure. For (C) the solution content is 1.6 wt.% PEDOT:PSS mixed with 5wt% to 20wt% DMSO (and 1 wt.% Lycra) in water solution, with solution temperature of 40 °C. For (D) 1.6 wt.% PEDOT:PSS mixed with 10wt% DMSO in water solution but with different solution temperature was used. And (E-G) are SEM figures of the original dip-coated yarn with coating condition of : 1.6 wt.% PEDOT:PSS mixed with 10wt% DMSO in water solution, under 40 °C, coated for 1 hour.

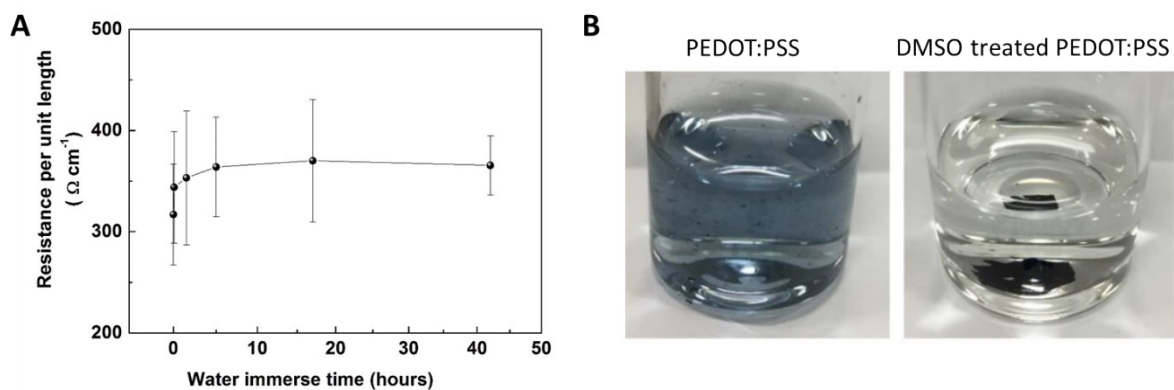


**Figure S2. The wet stability of PY.** (A) Unit length resistance change with water immersing duration shows a relative constant electrical resistance of the coated yarn after 42 hours submersion in water. (B) Image of pure PEDOT:PSS and DMSO treated PEDOT:PSS films immersed in water indicates the presence of DMSO in the PEDOT:PSS improves its water-stability. It is because the PEDOT:PSS microstructural changes induced by the polar solvent, DMSO. Specifically, with PSS extracted by DMSO, hydrophobic nature of PEDOT-rich domains has been accentuated. This finding indicates the potential of utilizing current coated yarn in humid environments.

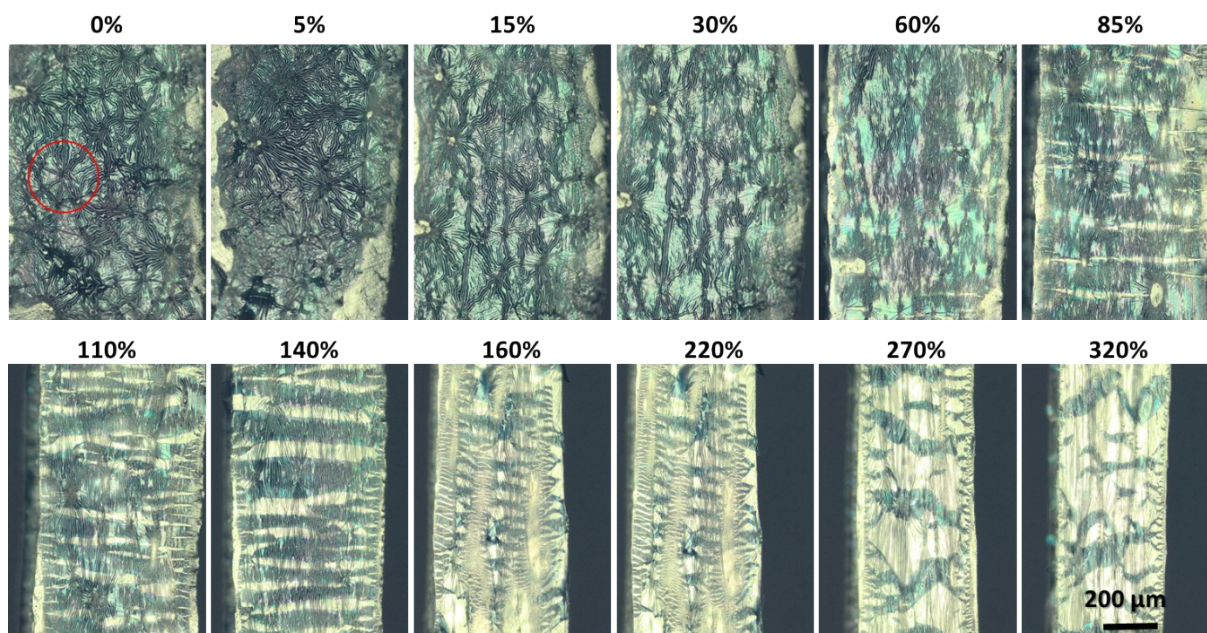


**Figure S3. The morphology of PEDOT:PSS coated Lycra® film.** Microscope images of the PEDOT-Lycra® film after the same swell-coating method as that for PY. Circular wrinkles of PEDOT:PSS as indicated by the red circle, prove the shrinkages during coating take place in both longitudinal and transverse directions of the yarns/films. Microscope pictures of the cracks induced under the different strains. Hot pressed Lycra® film were cut into strip and coated by PEDOT:PSS in the same method as fabricating PY.

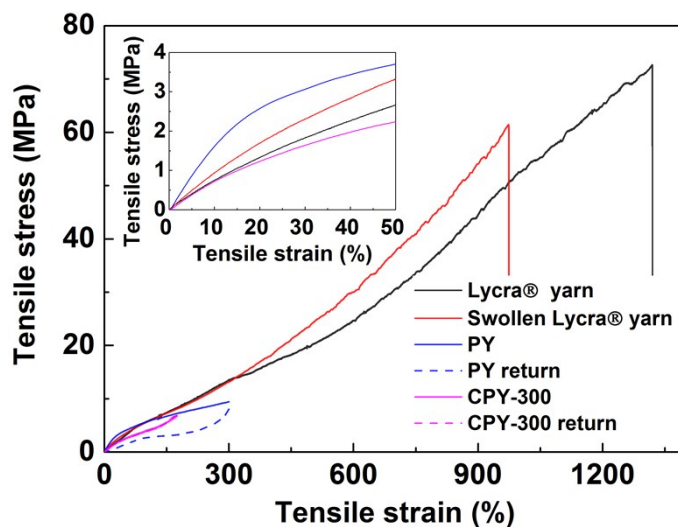


**Figure S4. Mechanical properties of Lycra yarn, PY and CPY.** Representative stress-strain curves for as-received Lycra® yarn, DMSO swollen Lycra® yarn dried in 120 °C oven for 2 hours, PY and CPY-300 and (insert) their performance at low strain. The stress is calculated by estimating the cross section as discussed in **Note S2**. The swollen Lycra® yarn shows a slightly higher Youngs’ modulus compared to pure Lycra®, as the swollen cross section area is slightly larger, while the same area value has been used for tensile stress calculation of both yarns.

**Table S1. Young’s modulus of Lycra yarns, PY and CPY.**

Sample	Lycra®	Swollen Lycra®	PY	CPY-300
Young’s Modulus	$7.5 \pm 0.1$ MPa	$8.3 \pm 0.5$ MPa	$16.6 \pm 1.3$ MPa	$7.8 \pm 0.6$ MPa

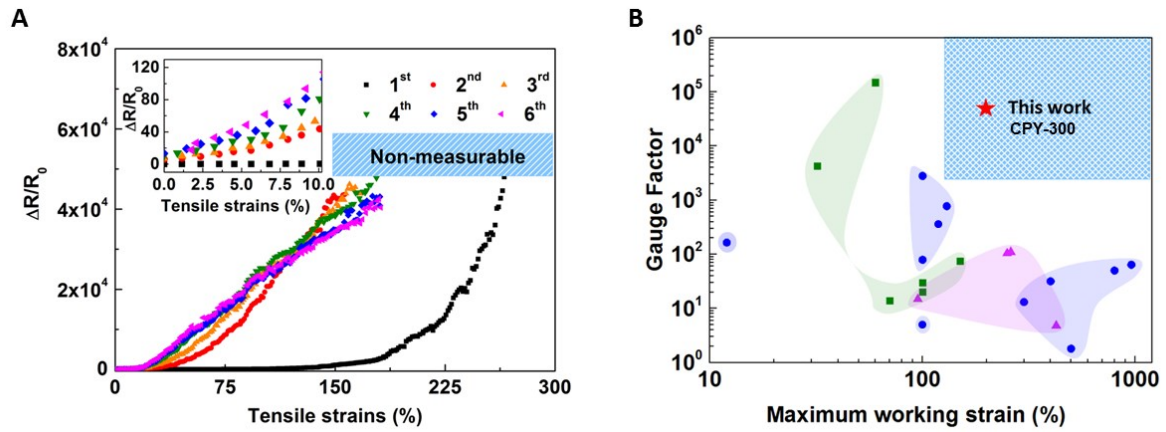


**Figure S5. Ultrahigh sensitivity to strain.** (A) Resistance change under different strains of all 6 times repetitions. PY was first stretched to 300% strain (after relaxation, it is called CPY-300) and the following stretch was cyclic strain to 200%. The inset shows the resistance change at low strains. (B) Comparison of the performance (maximum strain range and maximum GF) of recently reported strain sensors. Our work, especially CPY-300, shows extremely high stretchability and sensitivity in the challenge region (highlighted)<sup>2-19</sup>. The green, blue and purple shading indicates sensors based on graphene, carbon nanotube and conductive polymer, respectively.

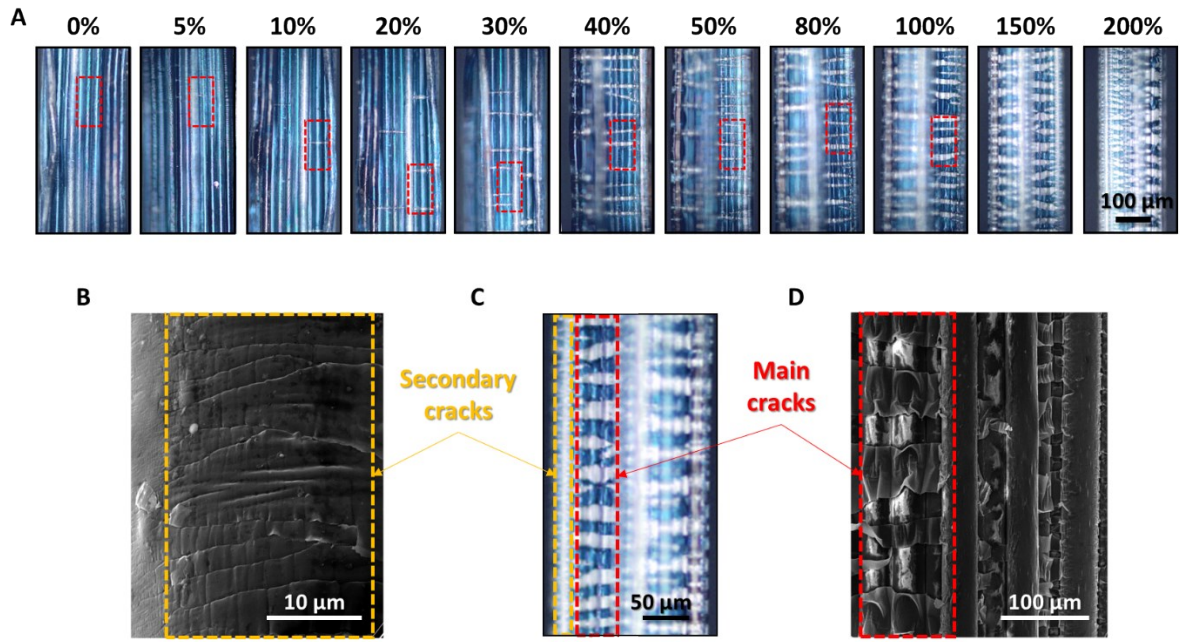


**Figure S6. The PY's cracking distribution under different strains.** (A) Original figures of **Figure 2A** in main text is the zoom in of the red dash box regions. And the SEM pictures show the secondary cracks (B) after relaxing from 300% strain and main cracks (D) under 300% strain, with (C) the secondary and main cracks distribution on the yarn as a presentative (strain ~150%) microscope picture shown.

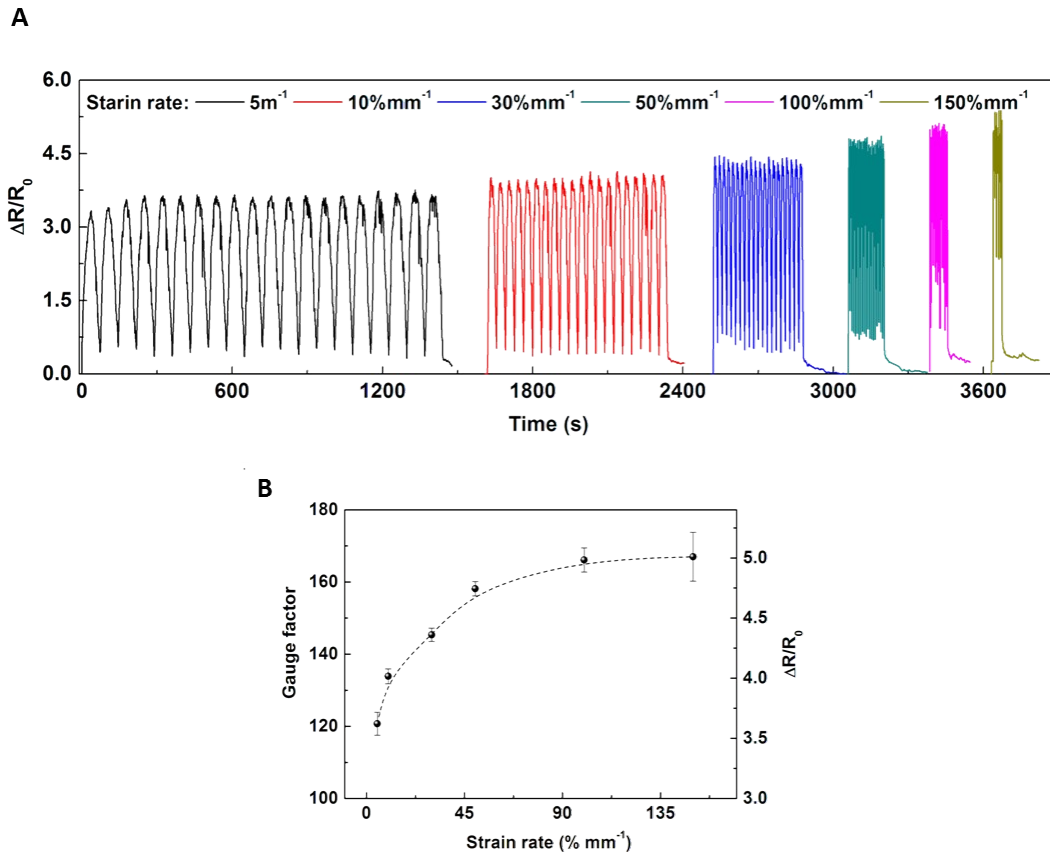


**Figure S7. The strain rate effect to sensitivity.** (A) The resistance change of CPY with the cyclic 3% strain under different strain rates and (B) their corresponding GF value.

## Note S1 - Calculation the interfacial shear strength

### By critical length

The critical length ( $l_c$ ) is defined as the minimum length of the PEDOT patches for a given thickness ( $t$ ) which will allow the tensile failure of the PEDOT layer rather than shear failure at interface, i.e., the minimum length the patches are able to crack by reaching the fracture stress.

As PEDOT:PSS is much stiffer than the Lycra® yarn, the Kelly-Tyson model can be applied, in which the matrix is simplified as an ideally elastic material. Also, it can be considered as an iso-strain situation, where the direction factor of the patches will be equal to 1.

Under the given loading, the shear effect build up from the patches ends where a plastic displacement zone exists. The stress carried increases until it reaches a constant  $\sigma_p$  in the middle part of the patches. With the increase of the applied load, the strains of PEDOT coated Lycra® yarn keep increasing, resulting in a higher stress in the PEDOT layer and will reach the fracture stress at the maximum stress  $\hat{\sigma}_p$ . PEDOT film breaks where it reaches the ultimate strength at  $X_c$ . If the length of any fragment is less than  $2X_c$ , the tensile stress in this fragment can not reach the ultimate strength and it does not break anymore.

The equilibrium equation of tensile force in patches and shear force at interface is

$$wt(\sigma(x + dx) - \sigma(x)) = \tau(x) wl_c dx \quad \text{Equation 1}$$

Where the  $w$  is the patches width,  $\tau$  is the shear strength. And  $t$  is the thickness of the coated PEDOT:PSS layer. Therefore,

$$\tau(x) = t \left( \frac{d\sigma}{dx} \right) \quad \text{Equation 2}$$

the critical length  $l_c = 2X_c$  is termed and can be calculated as

$$l_c = 2 \hat{\sigma}_p t / \tau \quad \text{Equation 3}$$

The fragment size is convergent to 22  $\mu m$  as can be seen in **Figure 2D** in the main text. The critical length  $l_c$  of coated PEDOT:PSS layer can be given by  $l_c = L_p/K$ . The well-accepted value  $K = 0.75^{20}$  was used.<sup>21</sup> So  $l_c \approx 29 \mu m$ .

The  $\hat{\sigma}_p$  for PEDOT:PSS is 30 MPa under RH 40%, at the maximum strain at break  $\sim 3\%$ .<sup>22</sup> The thickness of PEDOT layer is using 500 nm as measured from SEM picture.

Therefore, based on the relationship between critical length and the interfacial shear stress, (Equation 3), the shear stress between the PEDOT layer and Lycra<sup>®</sup> yarn can be calculated as 1.4 MPa.

#### By Agrawal and Raj model

The brittle PEDOT:PSS coating on ductile Lycra substrate can also be applied by Agrawal and Raj (A–R) model. Therefore, the maximum interfacial shear stress,  $\tau$  can be simplified as <sup>23</sup>

$$\tau = \frac{\pi t \hat{\sigma}_p}{1.5 \times \hat{W}_c} \quad \text{Equation 4}$$

Where the  $W_c$  is  $\sim 23 \mu\text{m}$  as shown in main text **Figure 2C**. And by using the same value of  $t$  and  $\hat{\sigma}_p$  as calculating by critical length, the calculated  $\tau$  is also 1.4 MPa.

## Note S2 – Optimization of coating parameters

A 1.6 wt.% PEDOT:PSS solution, 5 minutes coating duration and 1-cycle coating was found to be the most suitable combination of parameters for conductive yarn strain sensors. In terms of coating solutions, for instance, a concentration above 0.8 wt.% is necessary to achieve electrical resistances over a specimen length of 1 cm sufficiently low ( $3.2 \pm 0.5 \text{ M}\Omega$  for 0.8 wt.% to  $330 \pm 35 \Omega$  for 1.6 wt.%, **Figure S8A**) to be measurable by a 2-probe test station (as described in **Experimental Section**).

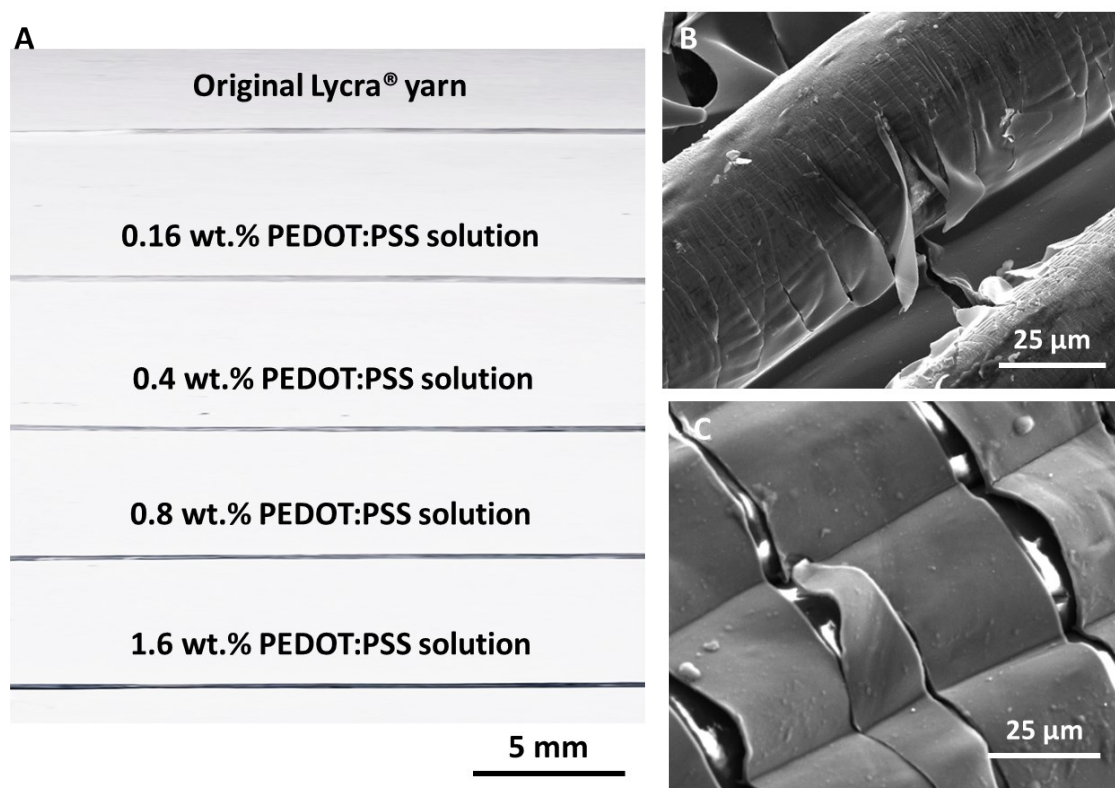


**Figure S8.** Images of PEDOT:PSS coated yarn by different parameters. (A) The digital pictures of Lycra® yarns coated within the different concentrations PEDOT:PSS in water solution. The concentration is achieved by diluting the as-purchased 1.6wt% PEDOT:PSS solution with DI water into different ratio. The higher the concentration of PEDOT:PSS solution, the more blue the yarns become, indicating more PEDOT:PSS deposited on the yarn. (B, C) SEM images of the stretched (B) 1-coating and (C) 3-coating cycle yarns. Thickness is obtained by measuring the cross section of PEDOT:PSS layer on cracked parts in SEM pictures.

The effect of coating time on the electrical resistivity presented **Figure S1A**, showing a decreasing trend with longer period of immersion, which is stabilized to a plateau beyond ~ 5 minutes. This is assumed to be related to the saturation of solvent exchange between PEDOT:PSS/water suspension and DMSO in Lycra® yarn. When more coating cycles are applied, the electrical resistivity of the yarn is further reduced, and no longer limited by the solvent exchange saturation (**Figure S1B**).

However, with increasing coating cycles, there is a trade-off between electrical properties and adhesion between PEDOT:PSS coating and substrate due to the large mismatch in their stiffness values, affecting subsequent crack patterning and electrical sensing properties. For example, after 3 coating cycles the yarn presents a thicker PEDOT:PSS coating (~1.5  $\mu\text{m}$ ), compared to the 1-cycle coating yarn (~ 300-500 nm), as measured from SEM images (**Figure S8b**). These values are in line with the thicknesses calculated from elastic Young's moduli of the different yarns (**Notes S3**). As expected, the highest electrical conductivity was found in the thickest yarn coating (115  $\Omega$  per cm length). However, as the number of coating cycles increased, the stiffness mismatch between the PEDOT layer and the ductile Lycra® yarn was also progressively and proportionally amplified, which, in turn, causes a permanent loss of conductivity when the yarns is stretched. This is due to the formation of extended and continuous cracks on the coating layer (separating isolated conductive coating 'patches'), propagated around the whole yarn and permanently disconnecting the electrical pathway.

Therefore, the 1-cycle for 5min in 1.6 wt.%PEDOT:PSS aqueous solution coated yarn has been employed for the research.

### Note S3- Calculations about PEDOT:PSS coating layer

#### Calculation of Lycra® yarn's cross section

Lycra® yarn as purchased is 940 dtex, and the density of the Lycra® yarn is between 1.15 g cm<sup>-3</sup> to 1.32 g cm<sup>-3</sup>, where 1.2 g cm<sup>-3</sup> is used for simplify calculation. The cross section has a circle shape, therefore, the cross section can be calculated by **Equation 5**.

$$A_L = \frac{940 \text{ dtex}}{1.2 \text{ g cm}^{-3} \times 10 \text{ km}} = 0.0783 \text{ mm}^2 \quad \text{Equation 5}$$

#### Calculation of thickness from the Young's modulus of the coating

The total force ( $F_T$ ) is the sum of the force on Lycra® ( $F_L$ ) and PEDOT ( $F_P$ ). In the meantime, the totally length change is same to the length change of Lycra® and PEDOT in the low strains within the elastic region ( $\varepsilon < 3\%$ ). Therefore, the PY system is equivalent to the two rods parallel system.

The PY's Young's modulus ( $E_{PY}$ ) is related to the Young's modulus of Lycra® ( $E_L$ ) and PEDOT ( $E_P$ ) along with the respective cross-sectional areas ( $A_L$  and  $A_P$ ) based on

$$E_{PY} = \frac{E_L A_L + E_P A_P}{A_L + A_P} \quad \text{Equation 6}$$

Here, the  $A_P$  is given by

$$A_P = 2\pi h \sqrt{\frac{A_L}{\pi}} = 2h\sqrt{A_L\pi} \quad \text{Equation 7}$$

If we combine the **Equations 6 and 7** the coated PEDOT thickness (h) can be calculated as

$$h = \frac{\sqrt{A_L}(E_{PY} - E_L)}{2\sqrt{\pi}(E_P - E_{PY})} \quad \text{Equation 8}$$

The values of  $E_{PY}$  and  $E_L$  are 16.6 MPa and 7.5 MPa as **Table S1** shows, and the  $E_P$  of 1.9GPa<sup>24</sup> has been used as reported at 40% RH. Therefore, the thickness of the PEDOT layer is 380 nm and is close to the results obtained from SEM measurements and observations.

As the moduli of the 2-5 times coated PYs are 27.8, 40.7, 24.5 and 25.6 MPa respectively, by using the same method, the thickness of the 2 and 3 times coatings are increasing to 850nm and 1400 nm, respectively. However the 4 and 5 times coated layers decrease to 710 nm and 630 nm, while the conductivity results in main text **Figure 1E** verified the coated PEDOT amount should higher than the 3 times coating. This means when coatings accumulate and stack into big flakes the PY is not fit to the parallel model anymore.

#### Calculation of the PEDOT:PSS coating amount based on coating thickness

Due to the difficulty to weight the amount of the PEDOT:PSS contain in the PY, for 1 layer PEDOT:PSS coated Lycra<sup>®</sup> yarn, the volume contain can be calculated by the geometry by equivalent the PY as a double-wall cylinder.

The volume ratios of the coated PEDOT:PSS in whole PY is  $\frac{A_P}{A_P + A_L} = 0.5 \text{ vol. \%}$ .

And based on the density  $\sim 1 \text{ g cm}^{-3}$  of PEDOT:PSS ( $\rho_P$ ) and  $1.2 \text{ g cm}^{-3}$  for Lycra<sup>®</sup> ( $\rho_L$ ). The

weight ratios for the PEDOT:PSS in whole PY is  $\frac{A_P \rho_P}{A_P \rho_P + A_L \rho_L} = 0.4 \text{ wt. \%}$ .

## Note S4- Understanding of the ultrahigh and tunable sensitivity

By increasing the pre-strain levels, the coating patches' length ( $L_p$ ) decreases while the crack width ( $W_c$ ) increases (Figure S9A). As Figure S9B shows  $L_p$  reaches the minimum length of  $\sim 22 \mu\text{m}$ , which we believe is related and analogous to a critical length value as calculated in Note S1.

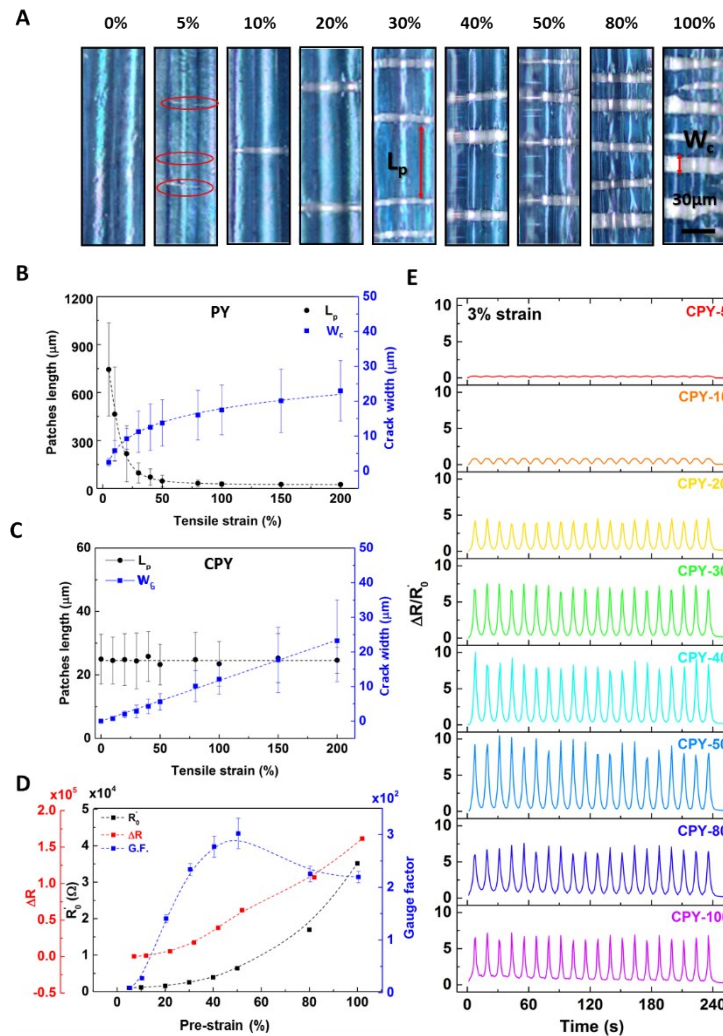


**Figure S9 Mechanism of ultrahigh and tunable strain sensitivity.** (A) Optical microscopy images of the PYs under different pre-strains, showing the crack development with pre-strain. (B) PY's and (C) CPY's crack width ( $W_c$ ) and patches length ( $L_p$ ) distribution under different pre-strains. (D) The effect of the pre-strain to the 0-position resistance ( $R_0$ , which is measured directly after pre-strain without relaxation), resistance variation with strain ( $\Delta R$ ) and gauge factor under cyclic loading (3% max strain). (E) The relative resistance variation ( $\Delta R/R_0$ ) of all the samples, CPY-5 to CPY-100, corresponding to the cyclic 3% strain.

The results of electrical strain sensing data, under cyclic tests up to 3% max strain, are presented in **Figure S9E** and summarized in **Figure S9D**. With an increased pre-strain value from 10% to 50%, both the resistance and the GF are significantly increased (from 8 to 302). This is likely due to the increased  $W_c$  and decrease in  $L_p$  from CPY-5 to CPY-50, with a much larger gap between conductive coatings. When further increasing the pre-strain to 100%, the GF slightly decreases to plateau at around 250. **Figure S9D** is the result of the initial resistance ( $R'_0$ ), which refers to the CPYs' resistance after 5 minutes relaxation from the pre-strain, monotonically increasing with pre-strain, and surpassing the resistance variation with strain ( $\Delta R$ ). It is worth noting that the increase of crack density is less pronounced when pre-strains are larger than 50%.

The electrical impedance response to a relatively wide range of frequencies can help to corroborate this explanation. Impedance spectra of PY and CPY at different strains were fitted with appropriate equivalent circuits. When PY is stretched for the first time (**Figure S10**), pure resistive behavior is dominating at low strains ( $\leq 20\%$ ). Initially, increasing strain causes an increase in the resistance, which is composed of contact resistance  $R_c$  and film resistance  $R_l$ . As cracks are developing at higher strains ( $\geq 30\%$ ), the impedance becomes frequency dependent. With further increased strain level, the cracks partially disconnect the conductive patches from each other, acting as capacitors. The combination of cracks and conducting paths are best described with a resistor  $R_l$  and a non-ideal capacitor or constant phase element ( $CPE_1$ ) in the equivalent circuit, with  $Z_{CPE} = 1/(T\omega^P)$  in parallel with the resistance of the contacts  $R_c$  in series (equivalent circuit in **Figure S9B**). The CPE with a P value close to 1 indicates a narrow distribution of the  $L_p$  and  $W_c$  values. The  $R_l$  resistance increases exponentially with strain and the capacitance decreases exponentially with strain (**Table S2**), due to the decrease in  $L_p$  and the increase in  $W_c$ .

After removing the initial deformation (from a 300% maximum strain), and upon reloading, the sample (i.e. CPY-300) shows a  $W_c$  which increases linearly with strain while the  $L_p$  is invariant (**Figure 8B**). At lower strains (5%), the yarn still behaves as a pure resistor as  $W_c$  is small and the coating remains electrically connected (**Figure S11**). However, the impedance becomes frequency dependent at a much earlier testing strain of 10%, compared 30% of the original PY, as the pre-cracked patterns are much easier to separate. At 10% strain, a high capacitance of 1030 pF is observed for CPY because the number of cracks of CPY at 10% strain is greater but its  $W_c$  is smaller than that of PY at the same strain. With increasing strain the cracks become wider and an increase in resistance and decrease in capacitance similar to PY is observed. It is interesting that after 50% strains, the behavior of CPY is rather different, as it is equivalent to two resistor and capacitor parallel combinations connected in series (as **Figure S11B**). Looking into the crack's morphology formed upon pre-strain (**Figure S6**), some secondary cracks ( $L_p$  and  $W_c$  smaller than 5  $\mu\text{m}$ ) exist between the major cracks along the yarns. The same can be observed in the case of a differently shaped substrate (i.e. a solution casted Lycra® film substrate, as shown in **Figure S3**). These secondary cracks develop as a result of the main cracks propagating into one another, particularly in slightly thinner parts of the coating, as well as at the edge regions. They act as a resistor connected in series or parallel to the main PEDOT:PSS cracked patches, allowing the electrically conductive pathways to remain connected. We believe that this can explain why PY and CPY remain conductive even at high strains. However, during the second stretch, at above 50% strain, these secondary cracks are much easier to be separates and a capacitive behavior is manifested as the distance between the small PEDOT:PSS patches is large enough. Therefore, a secondary resistance-capacitor parallel combination is added to the equivalent circuit model. With the strain increasing, the secondary capacitance is increasing linearly due to the total length of small cracks also increasing (**Table S3**).

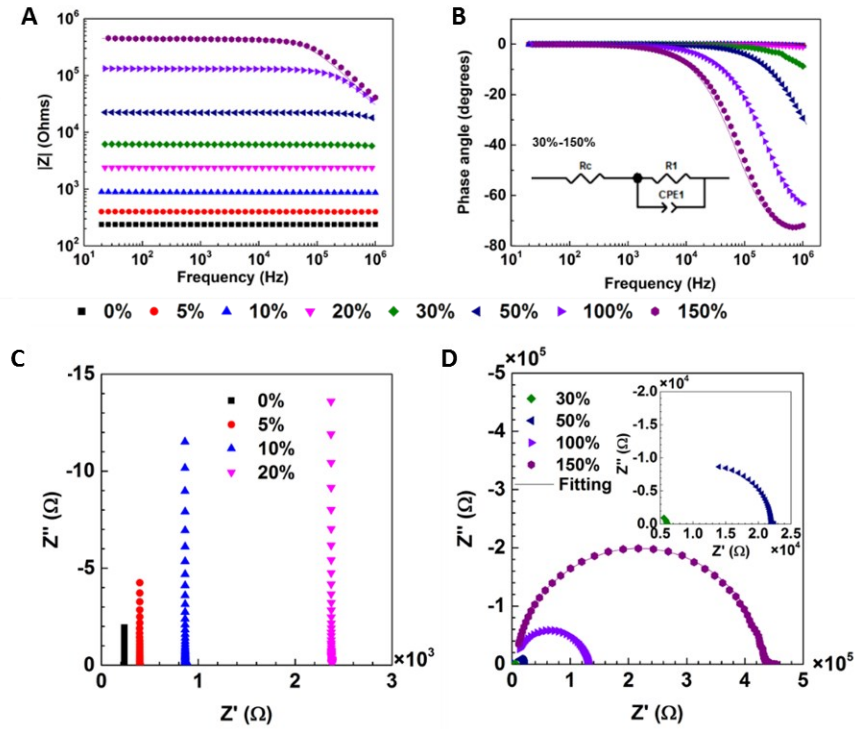


**Figure S10.** Impedance spectroscopy of PY. The frequency dependencies of the (A) moduli of the complex impedance ( $Z$ ) and (B) phase angle ( $\theta$ ), Nyquist plots at (C) low strain and (D) high strain, with fitted results (lines) based on a pure resistor ( $R_c+R_1$ ) model for lower than 20% strain and inserted equivalent circuit model for strain of 30% and above.

**Table S2.** Impedance parameters of PY as a function of different strains.

PY Strain	$R_c$ ( $\Omega$ )	$R_1$ ( $\Omega$ )	CPE1-T (pF)	CPE1-P	Chi-squared	Error
0%	237					0.015%
5%	397					0.029%
10%	870					0.066%
20%	2375					0.041%
30%	2574	3478	66.6	0.95	$4.06 \times 10^{-4}$	
50%	3520	$1.86 \times 10^4$	14.0	0.96	$8.69 \times 10^{-5}$	
100%	4768	$1.25 \times 10^5$	11.6	0.95	$7.28 \times 10^{-5}$	
150%	6764	$4.24 \times 10^5$	9.1	0.96	$1.41 \times 10^{-4}$	

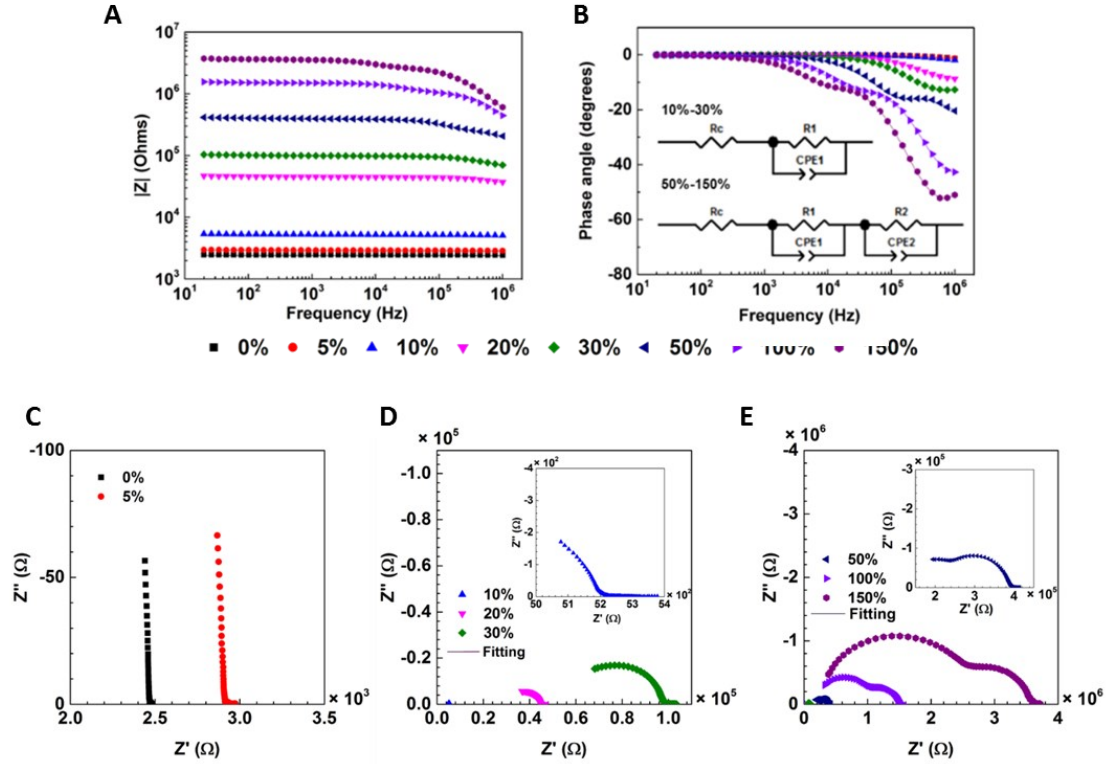


**Figure S11.** Impedance spectroscopy of CPY-300. The frequency dependencies of the (A) moduli of the complex impedance ( $Z$ ) and (B) phase angle ( $\theta$ ), Nyquist plots at (C) low strain, (D) medium strain and (E) high strain, with fitted results (lines) based on a pure resistor ( $R_c+R_1$ ) model for lower than 5% strain, and inserted equivalent circuit models for 10-30% strains and higher than 50% strains, respectively.

**Table S3.** Impedance parameters of CPY as a function of different strains.

CPY strain	$R_c$ ( $\Omega$ )	$R_1$ ( $\Omega$ )	$CPE_1$ -T (pF)	$CPE_1$ -P	$R_2$ ( $\Omega$ )	$CPE_2$ -T (pF)	$CPE_2$ -P	Chi-squared	Error
0%	2467								0.05%
5%	2922								0.08%
10%	456	4739	1030	0.89				$2.44 \times 10^{-5}$	
20%	$1.36 \times 10^4$	$3.12 \times 10^4$	103	0.87				$1.62 \times 10^{-4}$	
30%	$4.12 \times 10^4$	$5.68 \times 10^4$	44.7	0.88				$1.44 \times 10^{-4}$	
50%	$1.29 \times 10^5$	$1.08 \times 10^5$	1.28	1.00	$1.52 \times 10^5$	18.3	0.96	$2.65 \times 10^{-4}$	
100%	$1.92 \times 10^5$	$8.29 \times 10^5$	0.78	0.97	$4.76 \times 10^5$	36.2	0.93	$1.16 \times 10^{-4}$	
150%	$2.35 \times 10^5$	$2.27 \times 10^6$	0.86	0.94	$1.09 \times 10^6$	55.0	0.89	$2.47 \times 10^{-4}$	

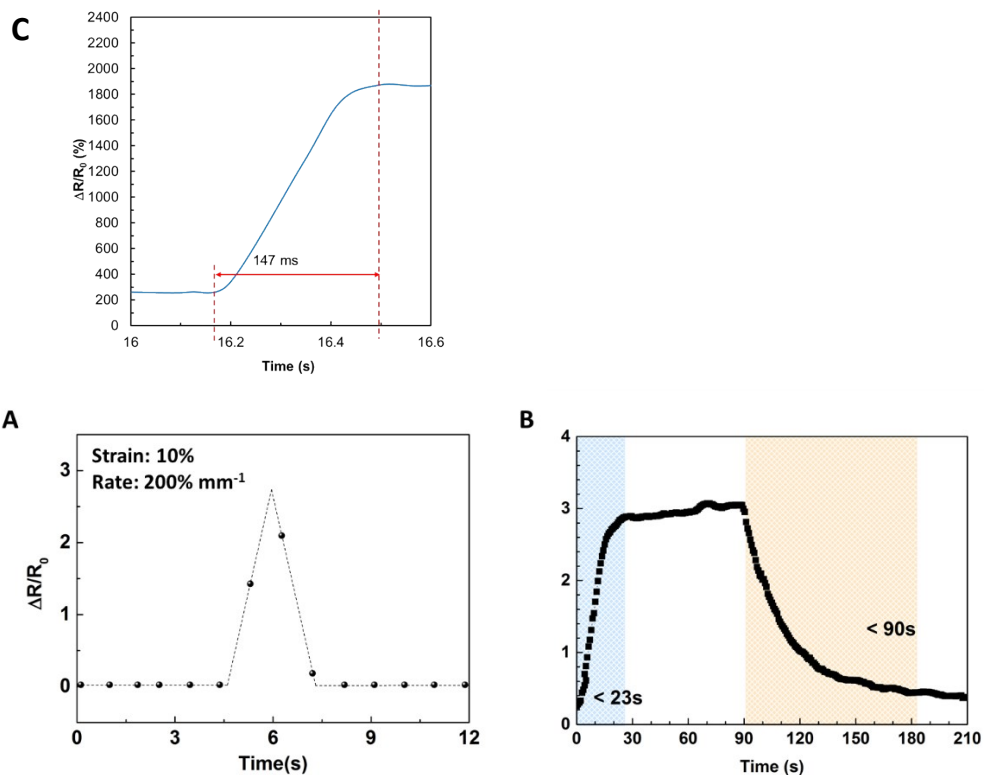


**Figure S13. (a) The response and recover time of the strain sensor is limited by the measurement system. The time of the whole response peak are close to 3 seconds which is very close to the strain time for the 10% strain under a 150% min<sup>-1</sup> strain rate. (b) The response time of the temperature sensor is smaller than 23 sec for 7k difference with a <90s recover time. C) Single cycle strain sensing test, carried out at higher acquisition rate, showing a response time in the order of tens of milliseconds.**

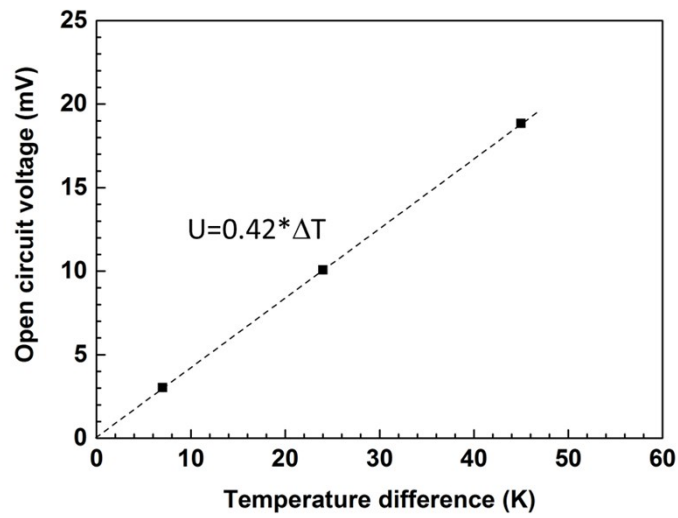


**Figure S14.** The relationship between open circuit voltage and temperature differences is linear.

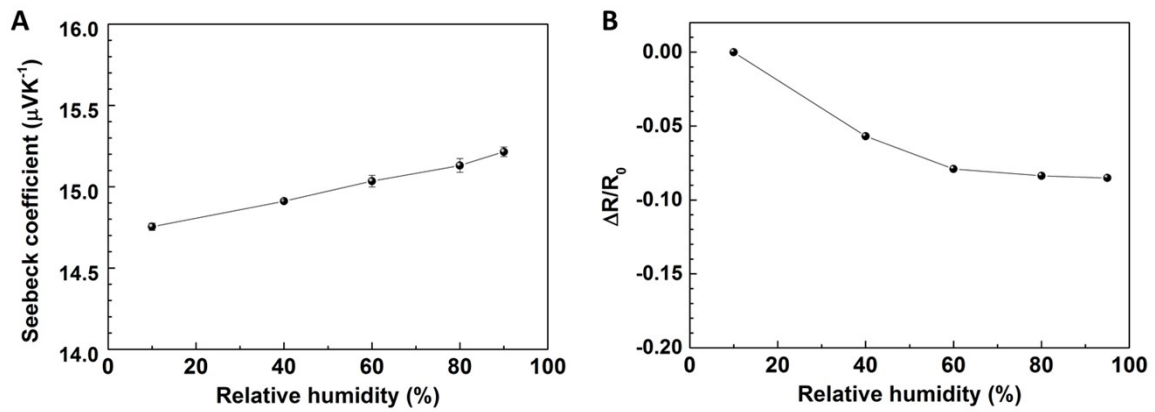


**Figure S15.** The sensor has a very small influence by the change of humidity on the (a) Seebeck coefficient and (b) resistance.

### Note S5 – Estimate the number of yarns for 10 $\mu$ W power output

The resistance of each yarn as p-leg with length of 5mm

$$R_p = 0.5mm * 330 \Omega cm^{-1} \approx 165\Omega$$

Resistance of each n-leg (constantan wires) with length of 5mm and diameter of 0.38mm is measured as  $R_n \approx 1\Omega$

Voltage output from per couple under 10  $^{\circ}$ C temperature difference

$$U_{p+n} = \Delta T \times (|S_n| + |S_p|) = 10 K \times (15 + 48)\mu V/K = 6.3 \times 10^{-4} V$$

And make the assumption of the contact resistance is 4  $\Omega$  for each p-n pair.

The number of the n & p couples (n) needed for 10  $\mu$ W is

$$P_{max} = \frac{(n \times U_{p+n})^2}{4n(R_p + R_n + R_{contact})}$$

$$n \approx 1.8k$$

Therefor only 1.8k pairs of yarn are needed for 10  $\mu$ W when  $\Delta T = 10$   $^{\circ}$ C.

## References

1. Y. Tao, Y. Liu, H. Zhang, C. A. Stevens, E. Bilotti, T. Peijs and J. J. C. Busfield, *Composites Science and Technology*, 2018, **167**, 24-31.
2. C. S. Boland, U. Khan, C. Backes, A. O'Neill, J. McCauley, S. Duane, R. Shanker, Y. Liu, I. Jurewicz, A. B. Dalton and J. N. Coleman, *ACS Nano*, 2014, **8**, 8819-8830.
3. S. Gong, D. T. H. Lai, Y. Wang, L. W. Yap, K. J. Si, Q. Shi, N. N. Jason, T. Sridhar, H. Uddin and W. Cheng, *ACS Applied Materials & Interfaces*, 2015, **7**, 19700-19708.
4. M. Amjadi, Y. J. Yoon and I. Park, *Nanotechnology*, 2015, **26**, 375501.
5. X. Xiao, L. Yuan, J. Zhong, T. Ding, Y. Liu, Z. Cai, Y. Rong, H. Han, J. Zhou and Z. L. Wang, *Adv. Mater.*, 2011, **23**, 5440-5444.
6. D. Kang, P. V. Pikhitsa, Y. W. Choi, C. Lee, S. S. Shin, L. Piao, B. Park, K.-Y. Suh, T.-i. Kim and M. Choi, *Nature*, 2014, **516**, 222-226.
7. N. Lu, C. Lu, S. Yang and J. Rogers, *Adv. Funct. Mater.*, 2012, **22**, 4044-4050.
8. E. Roh, B.-U. Hwang, D. Kim, B.-Y. Kim and N.-E. Lee, *ACS Nano*, 2015, **9**, 6252-6261.
9. Y. R. Jeong, H. Park, S. W. Jin, S. Y. Hong, S.-S. Lee and J. S. Ha, *Adv. Funct. Mater.*, 2015, **25**, 4228-4236.
10. C. Mattmann, F. Clemens and G. Tröster, *Sensors-Basel*, 2008, **8**, 3719-3732.
11. S. Gong, D. T. H. Lai, B. Su, K. J. Si, Z. Ma, L. W. Yap, P. Guo and W. Cheng, *Adv. Electron. Mater.*, 2015, **1**, 1400063.
12. J. T. Muth, D. M. Vogt, R. L. Truby, Y. Mengüç, D. B. Kolesky, R. J. Wood and J. A. Lewis, *Adv. Mater.*, 2014, **26**, 6307-6312.
13. J.-H. Kong, N.-S. Jang, S.-H. Kim and J.-M. Kim, *Carbon*, 2014, **77**, 199-207.
14. B.-U. Hwang, J.-H. Lee, T. Q. Trung, E. Roh, D.-I. Kim, S.-W. Kim and N.-E. Lee, *ACS Nano*, 2015, **9**, 8801-8810.
15. M. Amjadi, A. Pichitpajongkit, S. Lee, S. Ryu and I. Park, *ACS Nano*, 2014, **8**, 5154-5163.
16. M. Amjadi, K.-U. Kyung, I. Park and M. Sitti, *Adv. Funct. Mater.*, 2016, **26**, 1678-1698.
17. S. Han, C. Liu, X. Lin, J. Zheng, J. Wu and C. Liu, *ACS Applied Polymer Materials*, 2020, **2**, 996-1005.
18. J. Wu, Z. Wu, X. Lu, S. Han, B.-R. Yang, X. Gui, K. Tao, J. Miao and C. Liu, *ACS Applied Materials & Interfaces*, 2019, **11**, 9405-9414.
19. Z. Duan, Y. Jiang, S. Wang, Z. Yuan, Q. Zhao, G. Xie, X. Du and H. Tai, *ACS Sustainable Chemistry & Engineering*, 2019, **7**, 17474-17481.
20. T. Ohsawa, A. Nakayama, M. Miwa and A. Hasegawa, *Journal of Applied Polymer Science*, 1978, **22**, 3203-3212.
21. S. F. Zhandarov and E. V. Pisanova, *Mechanics of Composite Materials*, 1996, **31**, 325-336.
22. U. Lang, N. Naujoks and J. Dual, *Synthetic Metals*, 2009, **159**, 473-479.
23. S. Zhang, *Biological and Biomedical Coatings Handbook: Applications*, CRC Press, 2016.
24. U. Lang, N. Naujoks and J. Dual, *Synthetic Metals*, 2009, **159**, 473-479.
25. Z.-H. Ge, Y. Chang, F. Li, J. Luo and P. Fan, *Chemical communications*, 2018, **54**, 2429-2431.